

Variability in tidal harmonics of the coastal and estuarine waters of Goa during winter monsoon and spring inter-monsoon

Aditi Mitra, Sourav Mandal, P.R. Shanas, Duphrin Joseph, S. Yuvaraj, Jesbin George, P. Aravind, Jai Singh, V. Sanil Kumar*

Ocean Engineering, CSIR-National Institute of Oceanography
(Council of Scientific & Industrial Research), Dona Paula 403 004, Goa, India

*corresponding author Tel: 0091 832 2450 327 email: sanil@nio.org

Abstract

Harmonic analysis was carried out with simultaneously observed tide elevation in the coastal and estuarine regions of Goa. The tide elevations were consistent along the coastal stretch of 80 km; however, significant variations were obtained inside the estuarine channels. In both estuaries, the increase in tide elevation was observed from mouth to head, also reflected in the major harmonic constituents. M₂ was found to be the principal constituent, which was consistent in the coastal region. The maximum M₂ amplitude of 66.27 cm was recorded at Pontemol (upstream of Zuari estuary) during spring inter-monsoon. The increase of M₄ tide in both the estuarine channels confirms the non-linearity of the system. The phase lag of M₄ from the forcing tides of M₂ and S₂ indicated flood dominance of the system. The tidal current velocities were well-reflected by the tidal ellipse. Our datasets do not reflect significant changes in tidal dynamics in the two seasons. Instead, it was noticed that a small shift in bottom topography could lead to a considerable difference in the tidal dynamics of the system, which is reflected in the estimated form number and tidal skewness values. The study puts up an effort to compare the earlier harmonics with the present ones to infer the decadal evolution of the astronomical constituents in the estuarine stretch of Goa. Furthermore, the association between the larger wave with high water could indicate about the flood-risk of this region.

Keywords: Tide, Tidal constituents, harmonic analysis, Mandovi-Zuari estuary, Goa

1. Introduction

Ocean tides have previously been considered a stationary process since they are driven by the gravitational forcing of the Sun and the Moon (Cartwright and Taylor, 1971). However, long-term changes in the tides could be observed on regional as well as global scales (Woodworth, 2010; Mawdsley et al., 2014; Feng et al., 2015; Ross et al., 2017), leading to global mean sea level (MSL) rise (Church and White, 2011). Tidal changes are likely to alter several terrestrial changes such as the alteration in water depth, bottom friction, coastal morphology and stratification (Jay et al., 2011; Muller et al., 2012), which could eventually lead to sea-level rise. Tides could also lead to short-term alterations in MSL, which might manipulate extreme events such as storm surge or flooding in vulnerable coastal regions. Alterations in sea-level rise and coastal hydrodynamics could lead to sediment supply changes, which eventually result in erosion or accretion (Fan et al., 2018). Complex interactions between bathymetry, density gradient, tides and winds could result to vertical residual flow which would eventually lead to the health of an aquatic system. Among all the physical forces, tides play the major role in estuarine residual flow (Sigauque et al., 2021). Tidal forces, which are caused by the changes in the relative positions of the Sun, Earth and Moon, can cause a deformation of the earth leading to solid earth tide as well as ocean tide (Briciu et al., 2018; Zhou et al., 2021). Information on tides along the coast or estuary is vital to estimate tidal current and plan shoreline management (Kumar et al., 2011) and also as an input to a water quality model (Vijay et al., 2010). Various mechanisms are responsible for modulating and distorting the long tidal wave generated in the oceans and propagating towards the shallow seas or the shallower water of the bays and estuaries (Arjun et al., 2010).

Whenever the oceanic tides propagate into the shallow seas or estuaries, they generate high-frequency overtides which are important for the aquatic environment where tidal amplitude to water depth ratio is significant (Blanton et al., 2002). Therefore, tides must be decomposed into several harmonic constituents to get a clear idea of the non-linearity of the tidal forcing in the shallow seas. Hence, it is easy to analyze and explain the role of the major and minor constituents in the non-linearity of the tidal system. The tidal spectrum consists of a large number of major and minor constituents that are subjected to distortion while propagating from the ocean to the shallow areas (Manoj et al., 2009), and the distortion could be characterized by the non-linear growth of harmonics of the major astronomical constituents. The tidal range in upstream of estuary increases (decreases) due to the estuarine convergence (frictional damping) as the tidal wave propagates towards the shallow water region (Dyer, 1973; Song et al., 2016). The variation of amplitude and phase inside an estuarine channel is a factor of the incident shallow-water wave (tidal wave) at the mouth of the estuary and the

reflected wave generated by the propagation of the incident wave through the channel. The combination of complex geometry, strong tidal current along with high variation in bottom topography would stimulate the generation of non-linear tidal effects such as overtides and compound tides (Kang and Jun, 2003; Nidzeiko, 2010; Hosseini et al., 2016; Khosravi et al., 2017) e.g., due to the along channel changes of the tidal asymmetry, there is a spatial variability of the relative phase of M6 with respect to M2 (Blanton et al., 2002).

On the other hand, the generation of M4 tide is due to the progression of M2 component towards the estuarine environment (Hosseini et al., 2016). The asymmetry of tide elevation or tidal constituents inside the estuarine channel affects the topographical evolution of the estuary and, eventually, the navigability inside the channel. The tidal asymmetry together with the residual flow, might lead to the asymmetry in ebb and flood velocities (Hasan et al., 2011). The processes that influence the tide and tide-induced current are also helpful in flood protection (Prandle, 2009; Savenije, 2012). Therefore, several analytical and numerical studies have been undertaken in the nearshore region to determine the tidal propagation from offshore towards the estuarine channels. Earlier studies have also inferred that the tidal variations in estuaries are controlled mainly by the bottom friction and morphology of the channel (Jay, 1991; Friedrichs and Aubrey, 1994; Lanzoni and Seminara, 1998; Van Rijn, 2011; Garel and Cai, 2018).

There are several initiatives to understand the tides along the estuarine channels of Mandovi and Zuari, but the available studies are mostly based on the observations (Shetye et al., 1995; Manoj et al., 2009) and numerical approaches (Unnikrishnan et al., 1997). Researchers have also extensively studied this estuarine network's tidal propagation and freshwater influx by using a numerical model (Vijith et al., 2009; Vijith et al., 2016). However, simultaneous information from the coastal as well as in the estuary is crucial to understand the overall tidal propagation in this region and so far no initiative has been taken to understand the north-south variability of the tide elevation of this region which is crucial to have an overall idea of the physical characteristics of this region. Other than the estuarine system, the Port of Mormugao in Goa acts as an essential connector for mining and other industries as well as tourism. This region as a whole plays a pivotal role in the regional economy since the estuarine channels are used for transportation of iron and manganese ore to the port of Mormugao (Shetye et al., 1995; Manoj et al., 2009). The strategic location triggers the development of ports and harbours, land reclamation and several other activities which eventually impact the environment. Also, the increasing urbanization and population in the vicinity demand rapid engineering activities. Those require an understanding of the hydrodynamic processes of this region and a periodic and thorough impact assessment. Thus, understanding the tidal dynamics of the nearshore waters of Goa and estuary could

be useful for recreational and navigational purposes. Besides the economic importance, the area represents a typical network of the coast and estuary of the western continental shelf of India. Hence, the aim of the present piece of work was to understand the spatiotemporal variability of the tidal characteristics of this region. Also, this paper tries to determine the tidal asymmetry by various approaches such as form number, M4/M2 ratio and tidal skewness in this coastal and estuarine stretch. Hence, the present study puts an effort to discern the dynamicity of the coastal and estuarine waters of Goa. The study also tries to compare the present observation with previous observations to remark on the decadal variability. The study has attempted to answer the following questions: a) How does the tidal asymmetry change spatially and temporally? b) How much is the contribution of asymmetry from the harmonics into the total asymmetry?

2. Study Area

The 105 km long coastal stretch of Goa along with the major estuarine network of Mandovi and Zuari are chosen for the present study. The continental shelf width off Goa is 120 km and the shelf is nearly horizontal with a smooth surface and shallow gradient (Faruque and Ramachandran, 2014). This shelf is classified as a tropical open shelf. Along the west coast of India, several rivers are located that originate in the Western Ghats Mountain range and are connected with the Arabian Sea by shallow estuarine channels. The Western Ghats possesses an average height of 1000 m above MSL. The Mandovi and the Zuari are the two estuaries of the Mandovi-Zuari estuarine system and are situated along the coast of Goa which are connected by the Kumbarjua Canal (Fig. 1). The width of the Kumbarjua Canal is small enough to treat Mandovi and Zuari as two distinct estuarine systems (Vijith et al., 2016). Quite a few rivers join Mandovi where the Mhadei river is the major contributor of freshwater. The total river run-off of the Mandovi estuary during the monsoonal months is larger than the magnitude of the estuarine volume (Vijith et al., 2009). The average water depth in these two estuaries is around 5 m (Shetye et al., 1995). The cross-sectional areas of these estuaries decrease from mouth to head and the tidal influence could be noticed up to a distance of ~50 km from the mouth (Shetye et al., 1995). These estuaries are called monsoonal because they receive a heavy freshwater discharge (~400 m³/s) during the Indian summer monsoon (June-September); however, the flow in these channels is primarily tidal after the withdrawal of the monsoon (Shetye et al., 1995). Earlier studies revealed that the tidal amplitude in these channels remains unaltered in the first 40 km stretch from the mouth and a rapid decay is observed within the next 10 km (Shetye et al., 1995; Unnikrishnan et al., 1997). The estuarine network has been extensively used for the transport of goods (especially iron and manganese ore) for fishing and for dumping domestic and industrial sewage (Shetye et al.,

1995). Hence, five locations from the coast and four locations from each of the two estuaries are selected to understand the tidal characteristics of this region.

3. Materials and methods

Tide elevation data at different locations covering the coastal waters of Goa and the estuarine waters of Mandovi and Zuari are recorded for 30 days by tide gauges for two seasons; winter monsoon (25 November-26 December 2020) and spring inter-monsoon period (25 March-25 April 2021). Tide elevation was measured using Wave and Tide Recorder (WTR 9, Aanderaa Data Instruments, Norway). The data were recorded internally on a Data Storage Unit (DSU). Those data were recorded at every 30 minutes interval. Along with the tide measurements, currents are measured using single point Aanderaa (RCM9) current meters with resolution of 0.3 cm/s and acoustic frequency of 2 MHz. The RCM9 utilizes the well-known Doppler shift principles the basis for its measurements.

The locations and sampling periods are provided in Table 1. We could not obtain error-free data at three locations during the spring inter-monsoon period (viz. Panaji, Cortalim and Cundaim). Hence, those datasets are not included in the harmonic analysis. The observed sea-level data were applied for harmonic analysis by fitting a finite set of cosine functions having frequencies at the known astronomical forcing frequencies by the least square method. Tidal Analysis Software Kit (TASK) (Bell et al., 2000), developed by the Proudman Oceanographic Laboratory, UK, is used for the harmonic analysis and to separate the tidal and non-tidal components from the measured sea-level data. The analysis is performed with the help of 24 major constituents such as Q1, O1, M1, K1, J1, OO1, MU2, N2, M2, L2, S2, 2SM2, MO3, M3, MK3, MN4, M4, SN4, MS4, 2MN6, M6, MSN6, 2MS6 and 2SM6 (Kumar et al., 2011; Mitra et al., 2020). Further, the tide elevations are compared with the Topex-Poseidon (T/P) altimetry datasets and the global finite element solution model (FES2014) and based on that, the root mean square error (RMSE) and bias values are calculated. A tidal ellipse was plotted for each location to determine the tidal contribution in the total current using the T-tide module of MATLAB. The recorded surface current was resolved into the tidal u-v component to obtain the tidal ellipse. Tidal skewness was calculated to understand the tidal asymmetry and the contribution of tidal constituents in the asymmetry using the following formula:

$$Y_2 = \frac{\frac{3}{4} a_1^2 w_1^2 a_2 w_2 \sin(2\phi_1 - \phi_2)}{[\frac{1}{2}(a_1^2 w_1^2 + a_2^2 w_2^2)]^{\frac{3}{2}}} \quad (1)$$

$$Y_3 = \frac{\frac{3}{2}a_1w_1a_2w_2a_3w_3 \sin(\phi_1 + \phi_2 - \phi_3)}{[\frac{1}{2}(a_1^2w_1^2 + a_2^2w_2^2 + a_3^2w_3^2)]^{\frac{3}{2}}} \quad (2)$$

$$\beta_2 = Y_2 \left(\frac{a_1^2w_1^2 + a_2^2w_2^2}{\sum_{i=1}^n a_i^2w_i^2} \right)^{\frac{3}{2}} \quad (3)$$

$$\beta_3 = Y_3 \left(\frac{a_1^2w_1^2 + a_2^2w_2^2 + a_3^2w_3^2}{\sum_{i=1}^n a_i^2w_i^2} \right)^{\frac{3}{2}} \quad (4)$$

Total skewness = $\beta_2 + \beta_3$

Where a_i , w_i , and ϕ_i are the amplitude, frequency and phase of respective tidal constituents. The positive and negative values of the total skewness indicate the flood and ebb dominance, respectively. Here a total of six combinations are considered for the skewness estimation i.e. M2/M4, K1/O1/M2, M2/S2/MS4, M2/M4/M6, K1/M2/MK3 and M2/N2/MN4.

Channel convergence lengths of the two estuaries are calculated based on the following formula (Davies and Woodroffe, 2010):

$$B(s) \cong W e^{\frac{-s}{L_b}} \quad (5)$$

where, s = upstream arc length coordinate

$B(s)$ = channel width at s

W = mouth width of channel

L_b = distance over which the length of the channel reduces by a factor of e (~ 2.718282)

Datawell directional wave rider buoy is used for wave measurements at 12.5 m water depth for a period of 30 days each in the pre-monsoon and post-monsoon seasons. The buoy measure heave in the range of -20 to 20 m with a resolution of 1 cm and an accuracy of 3%. The buoy was deployed at Calangute on 25th November 2020 and 25th March 2021 at geographic locations ($15^\circ 31' 32.022''$ N; $73^\circ 45' 02.357''$ E) and ($15^\circ 30' 36.359''$ N; $73^\circ 44' 57.480''$ E) for post and pre-monsoon respectively. Reanalysis data of wind speed at 10 m height having one-hour interval were obtained from ECMWF ERA-5 (Herbasch et al., 2020).

4. Results

4.1 Variation of tide elevation in the coastal and estuarine waters

The tide elevations were found to be relatively invariable in the coastal locations. Maximum elevation was recorded as 2.5 m and 1 m during spring and neap, respectively, in both the seasons (Figs. 2 and 3). The tide elevations were different inside the Mandovi estuary, moving from mouth to

head during the winter monsoon. The elevations got increased around 0.5 m from Panaji to Khandepar (Fig. 4). In Akhada and Navelim, a shift in MSL was obtained, probably due to the drift of the tide gauge from the deployment location. In the second phase of observation, error-free data for Navelim and Khandepar were not obtained, and there was no amplification of tide between Panaji and Akhada (Fig. 5). Also, seasonal variability was insignificant in these two locations. Tide elevation was quite similar in the Zuari estuary as Mandovi (Fig. 6). MSL shift was noticed in Cortalim and Cundaim due to the drift of the instrument during the winter monsoon. The mean sea levels for the distinct elevation sections were estimated from the observed data. They were compared with the existing MSL magnitude to fix the sea level in the datasets. A small increase in tide from mouth to upstream could be seen in this case. Similar conditions prevailed during the spring inter-monsoon with no considerable amplification inside the channel (Fig. 5). In both seasons, tide elevation was found to be maximum at Pontemol (upstream of Zuari estuary).

4.2 Harmonic analysis of tide

4.2.1 Major constituents

Amplitude and phase of major constituents during winter-monsoon are represented in Fig. 7. The first section of Fig. 7 depicts the variation of major constituents inside Zuari from mouth to head. A general increasing tendency was observed from the mouth towards upstream except at Cundaim, where the amplitudes had a comparatively lower value than the mouth (Cortalim). The scenario changes in the case of Mandovi (middle panel of Fig. 7), where the amplitudes of the major constituents except M2 remain almost invariable. Even though the variation is small, there is a headward increasing trend in the case of M2. The situation is quite similar while considering the coastal locations where the amplitudes of each of the constituents remain invariable (rightmost panel of Fig. 7). The maximum magnitude was recorded in the case of M2, followed by K1, S2, O1 and N2. The phase variation inside the Zuari estuary was not uniform except for the major diurnal constituents (K1 and O1). In the case of M2, the phase was found to be invariable in the first three locations from the mouth, but a sudden drop was obtained between Rachol and Pontemol (Fig. 7). In the case of the Mandovi estuary, a higher magnitude of phase was obtained for the semi-diurnal constituents (M2, S2 and N2) in the mouth (Panaji), which had a sudden decrease inside the estuary (Fig. 7). The diurnal constituents were found to be invariable within the study region. The phase value of each of the constituents was found to be uniform in the coastal locations. However, the magnitudes were much higher in the case of the major semi-diurnal constituents.

Almost similar conditions prevailed during the spring inter-monsoon period (Fig. 8). An increase in M2 amplitude was noticed inside the Zuari estuary, which is not evident inside Mandovi. All other major amplitudes were found to be invariant within the estuarine system. There was a northward increasing trend in the case of the coastal amplitudes, which is the most significant for M2. Also, the phase variability is quite remarkable within the coastal stretch. S2 phase had a considerable drop at Majorda, which is not evident in the other three locations. Phase variation of all other constituents was not apparent in the case of the coastal locations. S2 phase had a decrease inside Zuari estuary, whereas no other phase varied; however, phase of O1 had a decrease between Panaji and Akhada.

4.2.2 Minor constituents

Among the minor constituents, the highest amplitude was noticed in case of Q1 during the winter-monsoon (Table 2). In the coastal region, the maximum magnitude was obtained in the central location (Majorda) and a gradual decrease towards south could be noticed. MU2 was the most dominating compound-tidal constituent at each location. Its magnitude was found to be invariable in the coastal stations. The amplitude of Q1 was quite invariable inside the Mandovi estuary except for Akhada, where a sudden decrease in magnitude was noticed. The most dominating over-tidal constituent was found to be uniform inside the Mandovi estuary except for the mouth (Panaji), where comparatively lower magnitude was encountered. The amplitude of Q1 was found to be undulating inside the Zuari estuary. The Q1 magnitude had a decrease from the mouth (Cortalim) to the middle estuary (Cundaim), and increased further upstream. A similar trend was obtained for the compound-tidal constituent MU2. The magnitude of MU2 in Cundaim was much higher (>10 cm) and was found to be greater than the major diurnal constituent O1. The variation in the phase of Q1 was found to be negligible inside Mandovi. The phase of MU2 was found to be very high at the mouth and got decreased inside. Similar results were obtained in the Zuari estuary. Almost similar conditions prevailed during the spring inter-monsoon period with minor variations in the dominant overtide and compound tidal constituents (Table 3).

4.3 Variations of tidal anomaly correlation/tidal form factor and M4/M2

The tidal anomaly correlation or the form factor did not have a spatial variation (Table 4) along the coastal and the estuarine extent. However, the magnitude indicated semi-diurnal dominance throughout the study region. The M4/M2 magnitude along the coastal stretch was found to be invariable; however, a marginal increase was obtained in the Mandovi estuary from mouth to upstream

(Table 4). On the contrary, amplification of M4/M2 could be seen in Zuari, especially in the Cundaim station. No seasonal variation was evident in this case.

4.4 Tidal Ellipse

The tidal ellipse, which is a diagnostic tool to understand the tidal currents of a region, is plotted for the available observed datasets at each location. The tidal velocities of the major constituent (M2) are well-reproduced by the tidal ellipse (Fig. 9). More or less rectilinear currents are observed for M2 at the coastal locations except for Calangute and Majorda. Estuarine stations, which are very near the river mouth, also have depicted similar currents that were no longer rectilinear inside the channel. The tidal current at Mandovi estuary was more linear than that of the Zuari. Clockwise currents were observed at each location except Cundaim.

4.5 Comparison of TOPEX Altimetry Data

The observed tide elevation data were compared with the TOPEX-Poseidon (T/P) and FES2014 altimetry data retrieved for the study region (Table 5). The altimeter data showed a good match with the observed; however, data could not be recovered for the estuarine locations other than Cortalim and Cundaim in the case of TOPEX. On the other hand FES2104 could not retrieve data from any of the estuarine locations. At Majorda, underestimation of the tide values in TOPEX altimetry data is noted.

4.6 Tidal skewness and channel convergence

To quantify the tidal asymmetry over the coastal and estuarine region, skewness was quantified. It could very well capture the amplitude and phase information of any time-series data. The entire coastal stretch has depicted flood dominance during the winter monsoon period, whereas during the spring inter-monsoon period, Calangute and Polem have indicated ebb dominance (Fig. 10). The estuarine locations observe distinct skewness characteristics, wherein the upstream of both Mandovi and Zuari estuary, ebb dominance could be noticed during the winter monsoon period. However, comparatively better flood dominance was encountered during the spring inter-monsoon season. The skewness contribution from the K1, O1, M2 combination was found to be the maximum irrespective of the spatial or temporal variability. The channel convergence length of Mandovi and Zuari estuary is calculated based on Eq. (5) were found to be 23.41 km and 13.38 km, respectively, indicating stronger convergence in Zuari.

4.7 Variability of wind and wave

The wind data near Calangute for the two seasons were obtained from ECMWF datasets and the maximum wind speed was found to be 8 m/s and 12 m/s during winter monsoon and spring inter-monsoon seasons (Figs. 11a and 11b). The measured wave data is processed, and the derived wave characteristics (significant wave height, mean wave period and wave direction) are presented in Figs. 11c to 11h. During winter-monsoon measurement, the significant wave height for the Calangute region varies from 0.3 to 0.8 m, and the mean is around 0.5 m. The predominant wave direction is between 180 and 240°. The average zero-crossing mean wave period for the measurement period is approximately 4.9 s, while mostly it varies from 3 to 9 s. However, during the spring inter-monsoon measurement period, it is found that the average significant wave height is around 0.6 m, and it varies from 0.4 to 2.5 m. The wave direction mainly persisted between 200 and 240°. The mean wave period varies between 3 to 8 s, with an average mean wave period of 4.37 s. Since, the spatial variability of these parameters was not evident, a single coastal location was chosen to represent the entire region.

5. Discussion

5.1 Tidal Harmonics and non-tidal residues

The measured tide elevations revealed that tide heights were mostly invariable along the 80 km long coastal stretch of Goa; however, there were changes inside the estuarine channels. Due to the convergence inside the estuarine channel, slight amplification in the tidal amplitude was noticed from mouth to head. There is a noticeable impact of MSL in the tide elevation of the estuarine channel. When the moored instruments were drifted from the respective deployment locations due to the dragging by fishing vessels, an immediate reflection is evident in the MSL, which eventually impacted the tide elevation. In general, changes in the atmospheric pressure and the wind stress are the major factors to modulate the MSL (Wouters et al., 2011; Amiruddin et al., 2015), but a change in the bottom topography could also lead to changes in the MSL of the estuary (Rasquin et al., 2020; Wachler et al., 2020). Tidal constituents followed a similar trend of variation as the tide elevation. M2 had the maximum amplitude throughout the study region, which is indicative of the dominance of the semi-diurnal tide. Even though the tide elevation did not vary much in the coastal region, variability was obtained in the major tidal constituents. Maximum M2 amplitude of 66.27 cm was noticed in Pontemol (upstream of Zuari estuary) during the spring inter-monsoon. M2 amplitude had a steady increase inside Mandovi, whereas considerable fluctuations were noticed in Zuari. S2 constituent was invariant at the coastal stations, but significant variability was obtained inside the estuaries. The amplification of M2 tide mainly contributes to the amplification in the tide elevation from mouth to head. The

principal overtidal and compound tidal constituents were M4 and MN4, respectively. The increase of M4 inside the estuarine channels confirms the non-linearity of the system. In a linear system, M4 would rapidly decrease from mouth to head within the channel (Aubrey, 1985). Amplification of neither the semi-diurnal nor the diurnal constituents was noticed along the coastal stretch. However, major semi-diurnal and diurnal constituents had an increase inside the estuarine channel. The amplification inside the Zuari estuary was higher than that of Mandovi, which is mainly due to the distinctive bathymetry and the channel convergence within these two estuarine stretches, which is well-reflected by the calculated index. The maximum tidal amplitude at Pontemol (upstream of Zuari) manifests the stronger channel convergence. This phenomenon is also reflected in the tidal ellipse, where currents were more rectilinear inside Mandovi than Zuari. An increase of the M4 magnitude inside both the channels confirms the non-linearity as well as the flood dominance inside the system. Also, the decrease in phase towards the upstream region signifies flood dominance in both the estuaries.

The wind and wave data together with the non-tidal sea-level indicated that the non-tidal residue in the coastal region is contributed by the wind. The maximum wave-height period in this region coincided with the period of maximum wind which is similar to the other regions from the west coast of India (Kumar et al., 2011; Kumar et al., 2012). Our data also manifested higher (lower) wave height during spring (neap) tide period which is associated with the high (low) water-level which could be applicable in the flood risk assessment (Lewis et al., 2019).

5.2 Tidal parameters

The variability in the estimated skewness indicates the tidal non-linearity in the region. During the winter-monsoon period, the ebb dominance upstream of the estuaries indicates the plausible impact of the river discharge in the tidal dynamics. The river flow constrains the saltwater intrusion and eventually enhances the ebb current (Horrevoets et al., 2004; Gallo and Vinzon, 2005; Guo et al., 2014). Nidzeiko (2010) has indicated that despite the ebb dominance at the mouth, estuaries could become flood dominant in upstream due to the non-linear distortion. During this season, the hydrodynamics is entirely dependent upon the river-tide interaction. However, during the spring inter-monsoon season, the estuaries behaved more flood-dominant due to the absence of the river discharge. The quarter diurnal compound tides include MS4, which is derived from the interaction of M2 and S2 constituents. The lag of MS4 from the forcing tides is indicative of the flood dominance of the system (Mitra et al., 2020). However, the amplitude of the compound tide was found to be much smaller than the parent constituents. Hence, its contribution to the total tidal energy balance is questionable. The study by Manoj et al. (2009) has revealed that due to the presence of mudflats in the upstream of Zuari

estuary, the ebb period increases, which makes Zuari a less flood dominant estuary than Mandovi. Recent studies have concluded that the presence of elevated mudflats could accelerate sea-level rise, which would eventually decrease the ebb dominance of the system (Wachler et al., 2020). Under the global climate change scenario, the increase in MSL is evident, which would probably have indirect impacts on the tidal channels. The flood dominance would disturb the estuarine self-clean-up and, eventually, the ecosystem. It could also enhance the landward supply of the suspended sediment (Guo et al., 2014), which would lead to an imbalance of the sediment budget of the estuary. However, in the case of the monsoonal estuaries, the freshwater influx during the Indian summer monsoon plays a key role in flushing out the estuarine water during the ebb, which eventually restores health. Numerical modelling studies have recorded meagre flushing time in Mandovi estuary during the summer monsoon (Manoj, 2012), which indicates the dominance of freshwater flow on the dynamics of the estuary during monsoonal months. The present study has also come across a similar result where the upstream of the estuaries became ebb dominant due to the presence of freshwater discharge in the winter monsoon.

The magnitude of the tidal form factor was found to be consistent throughout the study region. Comparatively lower magnitudes were dominated inside the estuarine channel, which indicates the dominance of semi-diurnal tides. An exception has been noticed in Cundaim, where a higher magnitude of form number is encountered. This could be explained by the sudden decrease of the semi-diurnal constituents in this location. Hence, the contribution from diurnal counterparts was found to be more. Overall, the magnitudes of the tidal form factor indicate that the tides in this region could be demarked as mixed and predominantly semi-diurnal in nature. The consistency of the amplitudes of the major constituents discards the frictional dominance inside the estuary, but the non-linearity of the amplitude and phase variations reveal the balance between pressure gradient and friction (Shetye et al., 1995). Also, the rapid increase of the first and second harmonics of M2 tide delineates the non-linear nature of the estuary (Manoj et al., 2009). The M4/M2 magnitude reveals rapid distortion of tide inside the Zuari estuary from mouth towards upstream, while this is not evident inside Mandovi. Overall, based on month-long tide elevation data, the present study infers negligible variation of the tidal dynamics on a temporal scale; however, spatial variability is evident in the estuarine stretch. Even though there is a small temporal variation in the constituent amplitude, significant variations were obtained in the estimated skewness. The calculated tidal ellipse data revealed the tidal origin of the water current in this region. The comparison between the ellipse-phase with that of the observed tide, has indicated that the maximum contribution of the tidal amplitude is from the M2 counterpart in the coastal region, whereas the contribution diminishes inside the estuary.

5.3 Comparison with the Global Models

Furthermore, the comparison of the tide elevation data with the T/P altimetry data has revealed that the predicted sea-level matched well with that of the observed for the coastal locations except for Majorda; however, it fails to predict the elevation in the upstream estuary region. The T/P data performed well in the mouth of the Zuari estuary. On the other hand, the elevation data of the coastal locations obtained from FES2014 better matched the observed data. However, elevations could not be retrieved at the estuarine locations. It is pretty evident that the global models are efficient in the deep-sea, but the inaccurate parameterization in the nearshore region leads to the erroneous prediction of the coastal sea level (Anderson et al., 1995; Shum et al., 1997; Cherniawsky et al., 2001).

5.4 Decadal Variability of Tidal Harmonics

Observed tidal amplitudes and phases of two selective locations of Mandovi (Akhada) and Zuari (Cortalim) were compared with the earlier data collected during 2003 (Table 6) to understand the decadal evolution of the harmonics. These datasets have revealed a significant change in the M2 phase inside the Mandovi estuary, where large decay in phase is obtained. On the other hand, substantial variation is not experienced in the Zuari estuary. In both the estuaries, an increase in the tidal phase is obtained for O1 in the present dataset. In the case of the amplitudes, major changes were encountered for the overtides MK3, MN4 and MS4 and for the compound tide M6, where an average two-fold decadal increase could be noticed. These could eventually be reflected in the long-term trend of the MSL. Previous studies have shown a rapid decay of tidal amplitudes after 40 km from the mouth, but the present study has not gone through such a phenomenon. These estuaries are strong converging channels; hence amplification was noticed from mouth to upstream, which is evident in the present study. Earlier studies have shown that the decay of amplitude in the upstream region is mainly due to the freshwater influx. Since the observations in the present case were taken during the winter monsoon and spring inter-monsoon seasons, the freshwater influx was negligible and hence, no rapid decay could be noticed in the upstream region.

6. Conclusion

The harmonic analysis revealed the non-linear nature of the Mandovi-Zuari estuarine system. Amplification of tide and major tidal constituents was noticed from mouth to upstream in the estuarine channels. The M4/M2 ratio indicates more substantial distortion inside Zuari than Mandovi. The study further elucidates that the change in bathymetry leads to a change in tidal dynamics. The measured data did not reveal any significant difference in the tide elevation and tidal harmonics along the coastal region of Goa in both seasons. The comparison with the global model data has led to accurate

prediction within the coastal stretch except for Majorda. The tidal ellipse data revealed that the system is tide-dominated and M2 was the major contributor to the tide elevation. The tidal skewness data indicated more ebb dominance in the upstream of the estuary during the winter monsoon; however, the estuaries were found to be flood dominant during the spring inter-monsoon season. The present result matches well with the earlier studies except for the compound and overtidal constituents. The average two-fold increase in amplitude was obtained within the last two decades. This study could provide crucial information for the management and mitigation measures in the shallow water region of Goa. Since the region is significant due to its geographic position for navigational and recreational purposes, continuous monitoring of the tidal hydrodynamics is required to understand the future of this region. Also, study integrating the wave climate and tidal dynamics is very much essential to demarcate the potential zones for natural hazards.

Acknowledgment: Director, CSIR-National Institute of Oceanography, Goa provided facilities to carry out the study. The authors acknowledge the financial support given by the National Institute of Ocean Technology, Ministry of Earth Sciences, Government of India to carry out the data collection. We thank all colleagues for the help provided during the field data collection. We thank both the reviewers for the suggestions which improved the scientific content of this paper. The first author wishes to acknowledge the Council of Scientific & Industrial Research, New Delhi for the award of a Senior Research Fellowship. This paper is a NIO contribution.

Data availability: The datasets generated during the current study are available from the corresponding author on reasonable request.

References

- Amiruddin, A.M., Haigh, I.D., Tsimplis, M.N., Calafat, F.M., Dangendorf, S., 2015. The seasonal cycle and variability of sea level in the South China Sea. *J. Geophys. Res.-Oceans*. 120, 5490—5513, <https://doi.org/10.1002/2015JC010923>.
- Andersen, O.B., Knudsen P., 1997. Multi-satellite ocean tide modelling—The K1 constituent. *Progress in Oceanography*. 40, 197–216.
- Arjun, S., Nair, S.L., Shamji, V.R., Kurian, N.P., 2010. Tidal Constituents in the Shallow Waters of the Southwest Indian Coast. *Marine Geodesy*. 33, 206–217, DOI: 10.1080/01490419.2010.495291
- Aubrey, D.G., Speer, P.E., 1985. A study of non-linear tidal propagation in shallow inlet/estuarine systems part I: observations. *Estuar. Coast. Shelf Sci*. 21, 185—205, [https://doi.org/10.1016/0272-7714\(85\)90096-4](https://doi.org/10.1016/0272-7714(85)90096-4).
- Bell, C., Vassie, J.M., Woodworth, P.L., 2000. POL/PSMSL Tidal Analysis Software Kit 2000 (TASK-2000). In: Permanent Service for Mean Sea Level, CCMS Proudman Oceanographic Laboratory, Bidston Observatory. Birkenhead, Merseyside, U.K. https://www.psmsl.org/train_and_info/software/task2k.php (accessed on 03/10/2018).
- Blanton, J.O., Lin, G., Susan A., Elston, S.A., 2002. Tidal current asymmetry in shallow estuaries and tidal creeks. *Continental Shelf Research*. 22.11-13, 1731-1743.
- Briciu, A.E., 2018. Diurnal, semi-diurnal, and fortnightly tidal components in orthotidal proglacial rivers. *Environmental Monitoring and Assessment*. 190-160 <https://doi.org/10.1007/s10661-018-6513-x>
- Cartwright, D.E., Tayler, R.J., 1971. New computations of the tide generating potential. *Geophys. J. Roy. Astron. Soc*. 23, 45–74, <https://doi.org/10.1111/j.1365-246X.1971.tb01803.x>.
- Cherniawsky, J.Y., Foreman, M.G.G., Crawford, W.R., Henry R.F., 2001. Ocean Tides from TOPEX/Poseidon Sea Level Data. *Journal of Atmospheric and Oceanic Technology*. 18, 649-664
- Church, J.A., White, N.J., 2006. A 20th century acceleration in global sea-level rise. *Geophys. Res. Lett*. 33, L01602, <https://doi.org/10.1029/2005GL024826>.
- Davies, G., Woodroffe, C.D., 2010. Tidal estuary width convergence: Theory and form in North Australian estuaries. *Earth Surf. Process. Landforms* 35, 737-749
- Dubey, K.M., Chaubey, A.K., Mahale, V., Karisiddaiah, S.M., 2019. Buried channels provide keys to infer Quaternary stratigraphic and paleoenvironmental changes: A case study from the west coast of India. *Geoscience Frontiers*. 10, 1577-1595
- Dyer, K.R., 1997. *Estuaries: a physical introduction*. Wiley, New York, 210
- Fan, Y., Chen, S., Zhao, B., Yu, S., Ji, H., Jiang, C., 2018. Monitoring tidal flat dynamics affected by human activities along an eroded coast in the Yellow River Delta, China. *Environmental Monitoring and Assessment*. 190-396, <https://doi.org/10.1007/s10661-018-6747-7>

- Faruque, B.M., Ramachandran K.V., 2014. Geological Society, London, Memoirs, 41, 213-220. <http://dx.doi.org/10.1144/M41.15>
- Feng, X., Tsimplis, M.N., Woodworth, P.L., 2015. Nodal variations and long-term changes in the main tides on the coasts of China. *J. Geophys. Res.-Oceans.* 120, 1215–1232, <https://doi.org/10.1002/2014JC010312>.
- Friedrichs, C.T., Aubrey. D.G., 1994. Tidal propagation in strongly convergent channels. *Journal of Geophysical Research.* 99, 3321– 3336. <https://doi.org/10.1029/93jc03219>.
- Gallo, M. N., Vinzon S. B., 2005. Generation of overtides and compound tides in the Amazon estuary. *Ocean Dyn.* 55, 441–448.
- Garel, E., Cai, H., 2018. Effects of Tidal-Forcing Variations on Tidal Properties Along a Narrow Convergent Estuary. *Estuaries and Coasts.* 41, 1924–1942, <https://doi.org/10.1007/s12237-018-0410-y>
- Guo, L., Wegen, M. van der, Roelvink, J. A. & He, Q. 2014. The role of river flow and tidal asymmetry on 1-D estuarine morphodynamics. *Journal of Geophysical Research: Earth Surface.* 119, 2315–2334, doi:10.1002/2014JF003110
- Hasan, G.M.J., Sebastiaan, D., Maren., V., Cheong, H.F., 2011. Improving hydrodynamic modeling of an estuary in a mixed tidal regime by grid refining and aligning. *Ocean Dynamics.* <https://DOI10.1007/s10236-011-0506-4>
- Horrevoets, A. C., Savenije, H. H. G., Schuurman, J. N., Graas S., 2004. The influence of river discharge on tidal damping in alluvial estuaries. *J. Hydrol.* 294(4), 213–228.
- Hosseini, S.T., Chegini, V., Sadrinassab, M., Siadatmousavi, S.M., Yari, S., 2016. Tidal Asymmetry in a Tidal Creek with Mixed Mainly Semidiurnal Tide, Bushehr Port, Persian Gulf. *Ocean Sci. J.* 51(2):195–208, <http://dx.doi.org/10.1007/s12601-016-0017-9>
- Jay, D.A., 1991. Green law revisited - tidal long-wave propagation in channels with strong topography. *Journal of Geophysical Research.* 96, 20585–20598. <https://doi.org/10.1029/91jc01633>.
- Jay, D.A., Leffler, K., & Degens, S., 2011. Long-term evolution of Columbia River tides. *ASCE J. Waterway Port Coast. Ocean Eng.* 137, 182–191, [https://doi.org/10.1061/\(ASCE\)WW.1943-5460.0000082](https://doi.org/10.1061/(ASCE)WW.1943-5460.0000082).
- Kang, J.W., Jun, K.S., 2003. Flood and ebb dominance in estuaries in Korea. *Estuar Coast Shelf Sc.* 56(1):187-196
- Khosravi, M., Siadatmousavi S.M., Vennell, R., Chegini, V., 2017. The transverse dynamics of flow in a tidal channel within a greater strait. *Ocean Dynamics.* <https://doi.org/10.1007/s10236-017-1127-3>

- Kumar, V.S., Johnson, G., Dora, G.U., Chempalayil, S.P., Singh, J., Pednekar, P., 2012. Variations in nearshore waves along Karnataka, west coast of India. *J. Earth Syst. Sci.* 121(2), 393–403
- Kumar, V.S., Dora, G.U., Philip, S., Pednekar, P., Singh, J., 2011. Variations in tidal constituents along the nearshore waters of Karnataka, west coast of India. *J. Coast. Res.* 27 (5), 824–829, <https://doi.org/10.2112/JCOASTRES-D-09-00114.1>.
- Lanzoni, S., Seminara, G., 1998. On tide propagation in convergent estuaries. *J. Geophys. Res.-Oceans.* 103 (C13), 30793–30812, <https://doi.org/10.1029/1998JC900015>.
- Lewis, M.J., Palmer, T., Hashemi, R. et al. 2019. Wave-tide interaction modulates nearshore wave height. *Ocean Dynamics.* 69, 367–384, <https://doi.org/10.1007/s10236-018-01245-z>
- Manoj, N.T., Unnikrishnan, A.S., Sundar, D., 2009. Tidal Asymmetry in the Mandovi and Zuari Estuaries, the West Coast of India. *Journal of coastal research.* 25(6), 1187–1197
- Manoj, N.T., 2012. Estimation of flushing time in a monsoonal estuary using observational and numerical approaches. *Nat. Hazards.* 64, 1323–1339, DOI 10.1007/s11069-012-0302-6
- Mawdsley, R.J., Haigh, I.D., Wells, N.C., 2014. Global changes in mean tidal high water, low water and range. *J. Coast. Res.* 70, 343–348, <https://doi.org/10.2112/SI70-058.1>.
- Mitra, A., Kumar, V.S., Jena, B.K., 2020. Tidal characteristics in the Gulf of Khambhat, northern Arabian Sea — based on observation and global tidal model data. *Oceanologia.* 62, 443–459, <https://doi.org/10.1016/j.oceano.2020.05.002>
- Müller, M., 2012. The influence of changing stratification conditions on barotropic tidal transport and its implications for seasonal and secular changes of tides. *Cont. Shelf Res.* 47, 107–118, <https://doi.org/10.1016/j.csr.2012.07.003>.
- Nidzioko, N. J., 2010. Tidal asymmetry in estuaries with mixed semi-diurnal/diurnal tides. *J. Geophys. Res.* 115, C08006, <https://doi.org/10.1029/2009JC005864>.
- Prandle, D., 2009. *Estuaries: dynamics, mixing sedimentation and morphology.* Cambridge: Cambridge University Press.
- Ross, A.C., Najjar, R.G., Li, M., Lee, S.B., Zhang, F., Liu, W., 2017. Fingerprints of Sea Level Rise on Changing Tides in the Chesapeake and Delaware Bays. *J. Geophys. Res.-Oceans.* 122, 8102–8125, <https://doi.org/10.1002/2017JC012887>.
- Rasquin, C., Seiffert, R., Wachler, B., Winkel, N., 2020. The significance of coastal bathymetry representation for modelling the tidal response to mean sea level rise in the German Bight. *Ocean Sci.* 16, 31–44, <https://doi.org/10.5194/os-16-31-2020>
- Savenije, H.H.G., 2012. *Salinity and tides in alluvial estuaries (2nd completely revised edition).* Available at www.salinityandtides.com (last access: 26 December 2014).
- Shetye, S.R., Gouveia, A.D., Singbal, S.Y., Naik, C.G., Sunder, D., Michael, G.S., Nampoothiri, G., 1995. Propagation of tides in Mandovi and Zuari estuarine network. *Proceedings of Indian Academy Sciences (Earth and Planetary Sciences).* 104, 667–682.

- Shum, C. K., Woodworth, P. L., Andersen, B., Egbert, G. D., Francis, O., King, C., Klosko, S. M., Le Provost, C., Li, X., Molines, J-M, Parke, M. E., Ray, R. D., Schlax, M. G., Stammer, D., Tiemey, C. C., Vincent, P., Wunsc, C. I., 1997. Accuracy assessment of recent ocean tide models. *J. Geophys. Res.* 102, 173–25
- Sigaúque, P.J., Schettini, C.A.F., Valentim, S.S., Siegle, E., 2021. The role of tides, river discharge and wind on the residual circulation of Maputo Bay. *Regional Studies in Marine Science.* 41, 2352-4855, <https://doi.org/10.1016/j.rsma.2020.101604>.
- Song, D., Yan, Y., Wu, W., Diao, X., Ding, Y., Bao, X., 2016. Tidal distortion caused by the resonance of sexta-diurnal tides in a micromesotidal embayment. *J. Geophys. Res. Oceans.* 121, 7599-7618, <https://doi.org/10.1002/2016JC012039>.
- Unnikrishnan, A.S., Shetye, S.R., Gouveia, A.D., 1997. Tidal propagation in Mandovi and Zuari Estuarine network, West Coast of India: impact of fresh water influx. *Estuarine, Coastal and Shelf Science.* 45, 737–744.
- Van Rijn, L.C., 2011. Analytical and numerical analysis of tides and salinities in estuaries; part I: tidal wave propagation in convergent estuaries. *Ocean Dynamics.* 61, 1719–1741. <https://doi.org/10.1007/s10236-011-0453-0>.
- Vijith, V., Shetye, S.R., Baetens, K., Luyten, P., Michael, G.S., 2016. Residual estuarine circulation in the Mandovi, a monsoonal estuary: A three-dimensional model study. *Estuarine, Coastal and Shelf Science.* 173, 79-92
- Vijith, V., Sundar, D., Shetye, S.R., 2009. Time-dependence of salinity in monsoonal estuaries. *Estuarine, Coastal and Shelf Science.* 85(4), 601-608
- Wachler, B., Seiffert, R., Rasquin, C., Kösters, F., 2020. Tidal response to sea level rise and bathymetric changes in the German Wadden Sea. *Ocean Dynamics.* 70, 1033–1052
- Woodworth, P. L., 2010. A survey of recent changes in the main components of the ocean tide. *Cont. Shelf Res.* 30, 1680–1691, <https://doi.org/10.1016/j.csr.2010.07.002>.
- Wouters, B., Riva, R.E.M., Lavallée, D.A., Bamber, J.L., 2011. Seasonal variations in sea level induced by continental water mass: First results from GRACE. *Geophys. Res. Lett.* 38, L03303, <https://doi.org/10.1029/2010GL046128>
- Zhou, M., Liu, X., Yuan, J., Jin X., Niu, Y., Guo, J., Gao, H., 2021. Seasonal Variation of GPS-Derived the Principal Ocean Tidal Constituents' Loading Displacement Parameters Based on Moving Harmonic Analysis in Hong Kong. *Remote Sens.* 13, 279. <https://doi.org/10.3390/rs13020279>

Table 1 Geographical position, depth and sampling period at the selected locations.

Location	Latitude/Longitude	Depth (m)	Period of recording	
			WM	SIM
Tiracol	15° 41' 40.04" N 73° 39' 54.66" E	12.0	25/11/2020- 26/12/2020	-
Calangute	15° 31' 32.02" N 73° 45' 02.36" E	12.5	25/11/2020- 26/12/2020	25/03/2021- 25/04/2021
Majorda	15° 17' 59.64" N 73° 52' 13.08" E	11.0	26/11/2020- 26/12/2020	25/03/2021- 25/04/2021
Cabo de Rama	15° 03' 47.55" N 73° 54' 50.08" E	14.0	26/11/2020- 26/12/2020	25/03/2021- 25/04/2021
Polem	14° 53' 57.84" N 74° 02' 15.36" E	11.0	26/11/2020- 26/12/2020	25/03/2021- 25/04/2021
Panaji	15° 30' 02.20" N 73° 50' 16.00" E	4.0	25/11/2020- 26/12/2020	24/03/2021- 08/04/2021
Akhada	15° 32' 22.00" N 73° 56' 08.40" E	4.2	25/11/2020- 26/12/2020	25/03/2021- 25/04/2021
Navelim	15° 30' 38.90" N 73° 59' 47.60" E	4.0	26/11/2020- 27/12/2020	-
Khandepar	15° 27' 12.90" N 74° 02' 26.70" E	5.0	26/11/2020- 27/12/2020	-
Cortalim	15° 24' 35.80" N 73° 53' 46.10" E	3.4	26/11/2020- 26/12/2020	25/03/2021- 25/04/2021
Cundaim	15° 26' 40.70" N 73° 56' 46.40" E	5.0	26/11/2020- 26/12/2020	-
Rachol	15° 19' 05.10" N 74° 00' 30.00" E	4.5	25/11/2020- 26/12/2020	-
Pontemol	15° 15' 16.80" N 74° 07' 40.80" E	3.6	26/11/2020- 26/12/2020	24/03/2021- 24/04/2021

Table 2 Variation of tidal constituents in the coastal and estuarine waters of Goa

Constituent	Coastal Stations												Mandovi river						Zuari river							
	Tiracol		Calanqute		Majorda		Caboderama		Polem		Panaji		Akhada		Navelim		Khandepar		Cortalim		Cundaim		Rachol		Pontemol	
	Amp. (cm)	Phase (deg)	Amp. (cm)	Phase (deg)	Amp. (cm)	Phase (deg)	Amp. (cm)	Phase (deg)	Amp. (cm)	Phase (deg)	Amp. (cm)	Phase (deg)	Amp. (cm)	Phase (deg)	Amp. (cm)	Phase (deg)	Amp. (cm)	Phase (deg)	Amp. (cm)	Phase (deg)	Amp. (cm)	Phase (deg)	Amp. (cm)	Phase (deg)	Amp. (cm)	Phase (deg)
Q1	3.9	75.8	3.6	79.3	4.3	76.4	3.9	76.7	3.7	81.6	3.4	86.7	2.6	111.4	3.3	120.4	3.6	119.4	3.3	89.6	1.9	92.4	3.1	76.6	2.8	102.0
O1	15.5	73.1	15.7	76.0	15.1	70.8	15.4	73.2	15.2	76.3	14.4	79.4	13.0	92.6	14.0	97.3	12.8	101.1	14.9	81.2	13.8	98.2	15.3	88.2	14.3	95.7
M1	0.4	36.3	0.5	52.7	0.4	26.8	0.5	44.1	0.5	54.5	0.7	82.5	0.8	113.7	0.5	122.5	1.7	121.8	0.7	50.6	1.3	195.4	1.4	87.9	1.2	122.3
K1	31.5	48.9	31.5	51.6	31.5	46.0	31.3	48.1	30.8	50.7	30.0	56.7	29.8	69.1	29.0	72.2	29.8	74.1	31.4	56.1	28.5	60.8	31.4	63.9	32.3	72.5
J1	2.0	74.1	2.0	78.2	2.1	64.7	1.9	66.9	1.9	67.0	1.8	87.3	1.1	115.6	2.8	141.7	2.2	167.8	2.0	66.1	4.5	114.2	1.0	161.2	2.1	141.3
OO1	1.4	79.7	1.6	82.9	1.3	74.5	1.5	80.1	1.6	91.1	1.0	53.3	1.8	17.2	1.0	50.0	1.6	356.5	1.5	85.4	1.8	311.3	1.3	16.9	1.3	344.0
MU2	2.3	290.7	2.4	302.2	2.3	287.5	2.2	290.4	2.2	301.8	0.6	328.0	2.1	107.0	2.4	101.4	2.4	128.3	1.9	320.9	10.1	117.7	3.1	84.2	4.7	108.7
N2	13.3	320.1	13.2	326.8	13.2	315.0	12.9	319.9	12.7	325.9	12.2	337.1	12.4	4.3	12.5	9.6	12.4	11.5	13.5	334.9	0.6	52.4	13.6	354.7	14.1	14.1
M2	53.6	326.8	53.6	332.7	53.6	321.9	52.5	326.8	52.2	332.5	51.9	341.3	54.8	5.5	57.9	11.1	59.6	10.8	56.4	340.5	43.7	341.1	61.6	353.5	65.5	11.3
L2	1.9	351.9	1.8	351.3	1.8	343.0	1.8	351.2	1.7	0.6	3.1	345.6	5.2	356.0	5.1	357.2	6.3	7.5	2.6	347.4	3.4	131.8	5.9	347.2	7.7	348.9
S2	21.0	337.6	20.7	343.8	20.8	332.9	20.3	338.5	20.1	344.7	18.3	354.5	17.4	26.0	18.0	32.2	17.8	31.7	20.7	354.5	15.9	6.8	20.2	9.7	19.9	36.9
2SM2	0.2	119.4	0.3	90.3	0.1	97.1	0.3	87.7	0.2	81.6	0.5	120.9	1.1	149.8	1.0	157.1	1.6	183.3	0.1	66.7	3.6	309.5	0.8	130.3	1.6	155.1
MO3	0.0	50.0	0.1	178.9	0.0	180.8	0.1	241.2	0.2	239.5	0.7	81.2	2.7	92.3	2.7	95.6	2.9	109.0	0.6	13.1	1.0	217.9	1.6	88.3	3.8	106.6
M3	0.5	332.1	0.4	344.9	0.4	323.3	0.4	316.8	0.3	315.1	0.3	4.9	0.5	338.1	0.9	356.3	1.2	28.7	0.4	1.6	2.5	111.9	1.1	47.5	1.2	38.4
MK3	0.2	265.5	0.1	97.4	0.1	100.0	0.1	157.3	0.1	84.8	0.3	62.7	1.7	43.1	2.2	61.3	1.7	59.9	0.1	48.0	3.9	170.9	1.7	144.1	2.3	129.0
MN4	0.8	26.0	0.8	40.8	0.9	12.7	0.9	23.9	0.9	31.0	0.4	68.9	0.7	200.7	0.7	218.5	1.6	221.9	0.8	58.3	1.8	155.5	1.5	161.3	2.0	207.6
M4	1.0	62.3	1.1	74.6	1.3	57.4	1.3	64.1	1.5	76.7	1.1	125.3	2.0	210.9	2.7	224.5	3.8	238.5	1.4	120.7	4.0	132.4	4.4	172.3	5.8	218.1
SN4	0.2	47.2	0.2	65.4	0.2	53.8	0.3	64.0	0.4	97.6	0.2	175.5	0.8	259.8	1.0	284.4	1.7	279.9	0.4	190.6	0.5	123.5	1.5	239.5	2.3	283.9
MS4	0.5	80.4	0.5	90.2	0.5	67.9	0.5	77.2	0.5	84.1	0.7	150.5	1.6	228.2	1.8	243.6	2.6	258.2	0.9	133.1	3.8	140.7	2.0	205.0	3.3	258.6
2MN6	0.1	316.0	0.1	14.9	0.1	302.4	0.2	304.6	0.1	316.1	0.4	334.1	0.7	36.2	1.0	71.1	1.3	83.4	0.2	340.1	0.2	192.3	0.6	24.5	1.2	80.7
M6	0.5	3.7	0.4	24.2	0.4	357.7	0.5	18.7	0.5	30.8	0.7	7.2	0.9	74.3	1.7	110.7	2.0	115.8	0.6	37.1	1.1	297.5	1.0	54.6	1.6	104.8
MSN6	0.2	26.1	0.2	39.9	0.1	20.1	0.2	47.3	0.3	71.7	0.2	30.6	0.4	118.1	0.5	129.8	0.7	155.7	0.1	23.7	0.4	295.1	0.5	57.0	1.0	130.5
2MS6	0.4	53.7	0.5	78.8	0.7	50.9	0.6	62.7	0.7	82.5	0.4	45.3	0.5	98.4	0.9	119.1	1.2	113.6	0.4	105.6	1.1	9.9	1.0	66.1	1.1	91.3
2SM6	0.2	115.7	0.1	123.2	0.2	47.4	0.1	122.3	0.1	121.8	0.0	45.8	0.2	103.9	0.2	115.4	0.4	95.2	0.2	153.8	1.3	15.6	0.2	89.2	0.6	113.3

Table 3 Variation of tidal constituents in the coastal and estuarine waters of Goa during spring inter-monsoon

Constituent	Coastal station						Mandovi				Zuari					
	Calagute		Maiorda		Caboderama		Polem		Panaji		Akhada		Cortalim		Pontemol	
	Amp. (cm)	Phase (deg)	Amp. (cm)	Phase (deg)	Amp. (cm)	Phase (deg)	Amp. (cm)	Phase (deg)	Amp. (cm)	Phase (deg)	Amp. (cm)	Phase (deg)	Amp. (cm)	Phase (deg)	Amp. (cm)	Phase (deg)
Q1	4.1	58.5	4.1	16.2	4.0	56.2	4.0	58.6	9.7	79.6	3.3	68.9	3.8	60.5	3.4	73.2
O1	16.4	49.0	15.6	283.0	15.4	48.3	15.3	52.1	5.3	347.4	14.0	61.2	15.4	54.0	14.1	64.1
M1	1.1	33.7	5.3	246.9	1.0	30.6	0.9	33.3	10.1	316.2	1.1	76.3	1.0	45.0	1.3	88.3
K1	34.0	55.3	32.0	350.3	31.7	54.7	31.4	58.2	41.9	103.4	31.8	76.9	33.2	61.3	35.4	85.1
J1	2.3	55.0	24.0	327.4	2.1	58.3	2.1	63.5	11.8	327.8	1.7	100.5	2.1	67.1	2.1	123.2
OO1	1.7	100.4	1.6	188.3	1.6	99.0	1.6	98.0	4.4	192.1	1.4	179.3	1.5	123.7	2.3	192.4
MU2	1.3	183.9	1.3	1.8	1.2	180.6	1.9	193.1	3.0	347.1	3.4	58.4	0.4	145.2	7.6	63.3
N2	13.5	281.2	12.1	313.5	12.6	279.9	12.9	284.7	11.6	278.1	12.8	326.3	13.5	295.7	15.1	349.1
M2	57.5	301.4	53.6	184.4	53.5	300.9	53.1	307.7	57.5	328.5	55.6	342.1	57.5	315.6	66.3	359.8
L2	1.7	316.3	1.6	295.3	1.7	318.2	2.6	330.4	9.6	342.2	4.1	297.0	2.2	309.8	7.8	299.5
S2	21.5	336.5	21.0	248.9	19.9	336.1	19.4	342.1	18.3	8.9	17.7	24.7	20.6	352.7	19.7	50.4
2SM2	0.2	94.6	30.3	285.5	0.2	73.9	0.5	246.8	0.6	306.5	1.1	217.4	0.4	166.9	2.5	222.2
MO3	0.1	135.9	0.3	178.7	0.1	99.4	0.1	145.4	0.7	46.6	1.8	38.1	0.4	15.7	3.4	76.6
M3	0.4	299.0	1.7	155.3	0.3	280.5	0.4	277.1	0.3	42.0	0.6	28.5	0.5	341.0	1.1	72.2
MK3	0.1	275.0	1.7	206.7	0.1	286.0	0.2	326.9	0.2	355.4	1.5	322.7	0.3	272.0	2.1	333.2
MN4	0.9	338.4	0.3	322.9	0.9	334.6	1.1	342.5	0.8	45.4	1.2	131.6	1.0	23.3	3.3	185.4
M4	1.2	18.1	0.4	137.9	1.3	20.4	1.4	33.7	0.5	78.3	1.8	156.0	1.5	64.3	5.0	191.6
SN4	0.4	332.8	0.5	73.7	0.4	341.9	0.4	353.4	0.5	159.7	0.4	338.4	0.4	335.6	1.2	325.7
MS4	0.9	62.4	0.6	100.3	1.0	64.5	1.1	76.2	0.5	95.2	1.6	228.2	0.9	116.1	3.2	259.0
2MN6	0.2	288.2	1.1	295.2	0.2	301.6	0.2	321.1	0.9	295.3	0.8	352.2	0.3	300.0	1.4	45.9
M6	0.3	277.6	0.7	207.0	0.3	287.7	0.3	314.6	0.8	163.2	1.1	358.5	0.5	297.0	1.9	64.4
MSN6	0.2	328.6	0.3	117.0	0.2	322.1	0.3	348.5	1.4	34.1	0.6	17.1	0.3	332.5	0.9	113.7
2MS6	0.7	13.8	1.1	284.5	0.8	32.8	0.9	59.7	0.8	306.5	1.2	39.2	0.6	42.9	1.8	103.2
2SM6	0.2	95.6	0.4	145.0	0.2	104.7	0.2	141.7	0.4	30.5	0.5	69.4	0.0	300.2	1.1	137.3

Table 4 Spatial variation of tidal form factor and M4/M2 ratio within the study region

Location	Winter monsoon		Summer inter monsoon	
	Tidal form Factor	M4/M2	Tidal form Factor	M4/M2
Tiracol	0.63	0.019	-	-
Calangute	0.63	0.020	0.64	0.02
Majorda	0.62	0.023	0.63	0.02
Caboderama	0.64	0.024	0.64	0.02
Polem	0.64	0.028	0.64	0.03
Panaji	0.63	0.020	0.62	0.01
Akhada	0.59	0.037	0.62	0.03
Navelim	0.57	0.047	-	-
Khandepar	0.55	0.064	-	-
Cortalim	0.60	0.025	0.62	0.03
Cundaim	0.71	0.09	-	-
Rachol	0.57	0.072	-	-
Pontemol	0.54	0.089	0.58	0.08

Table 5. Correlation (r), bias, Root Mean Square Error (RMSE) between TOPEX/POSEIDON or FES2014 tide and observed tide

Statistical Parameters	Predicted and observed tide											
	Tiracol		Calangute		Majorda		Caboderama		Polem		Cortalim	Cundaim
	T/P	FES2014	T/P	FES2014	T/P	FES2014	T/P	FES2014	T/P	FES2014	T/P	T/P
r	0.9	0.9	0.85	0.9	0.7 5	0.8	0.8	0.8	0.7 0	0.8	0.65	0.70
Bias (cm)	-0.04	-0.02	-0.04	-0.02	- 0.3 6	-0.03	-0.07	-0.03	- 0.0 8	-0.02	0.02	0.02
RMSE (cm)	0.07	0.05	0.04	0.03	0.0 7	0.06	0.05	0.03	0.0 7	0.05	0.07	0.06

Table 6. Comparison of observed tidal constituents with that during 2003

Constituent	Location							
	Akhada				Cortalim			
	2003		Present		2003		Present	
	Amplitude (cm)	Phase (deg)	Amplitude (cm)	Phase (deg)	Amplitude (cm)	Phase (deg)	Amplitude (cm)	Phase (deg)
O1	14.5	60.8	12.95	92.62	14.7	62.6	14.92	81.18
K1	34.1	75	29.78	69.07	35.5	63.0	31.37	56.11
N2	12.8	329.1	12.38	4.31	12.3	292.3	13.47	334.87
M2	55.3	345.5	54.83	5.48	59.9	319.6	56.35	340.50
S2	17.9	32.5	17.38	25.95	19.8	3.1	20.68	354.45
M4	1.2	284.8	2.02	210.91	2.7	117.1	1.35	120.65
M6	0.9	5	0.91	74.27	0.4	284	0.64	37.06
MK3	1.0	326.9	1.72	43.07	0.8	47.4	0.14	47.98
MN4	0.1	284.8	0.69	200.66	1.2	77.7	0.80	58.26
MS4	0.6	253.4	1.60	228.21	0.5	136.8	0.86	133.09

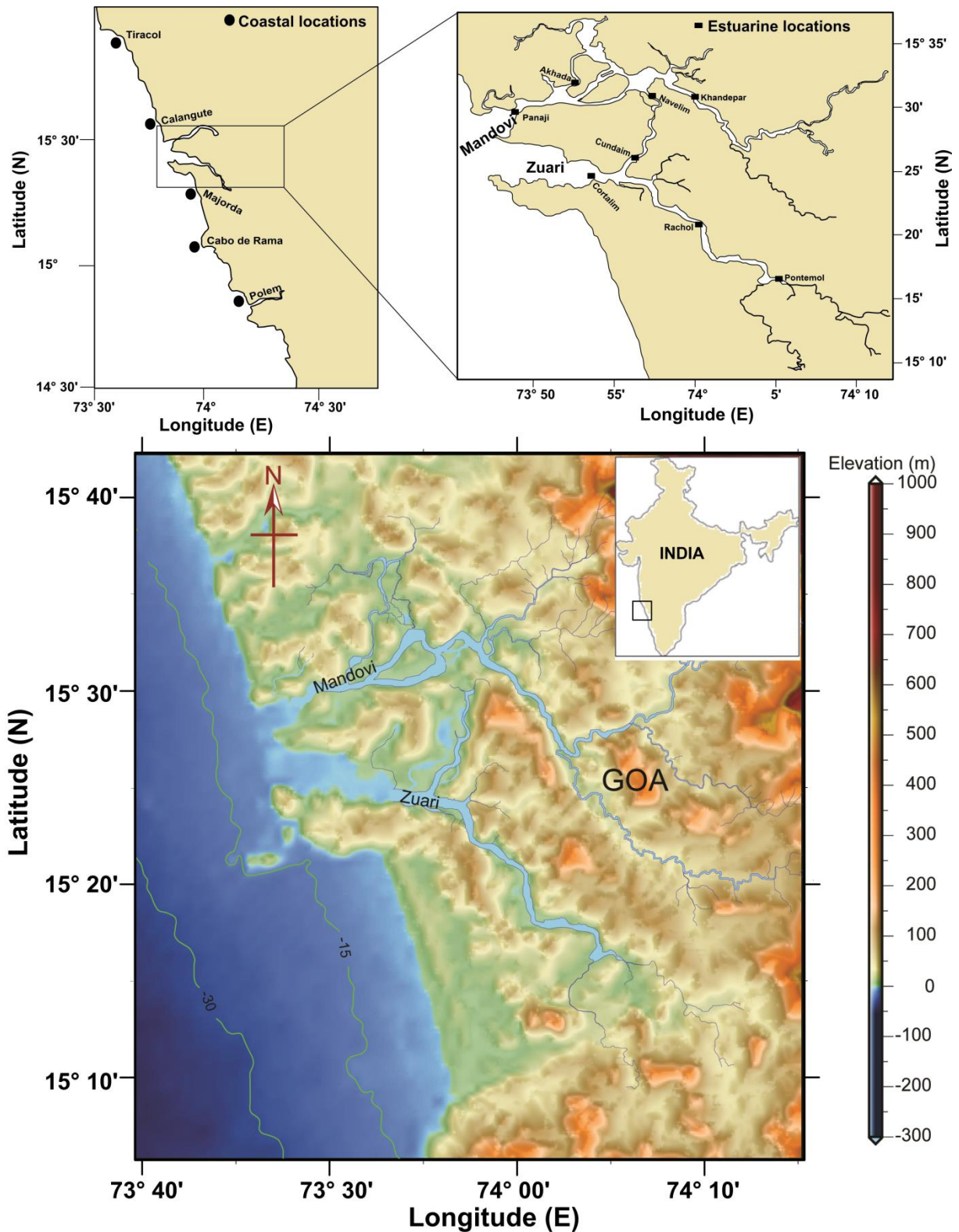


Fig. 1. Station locations around the coastal and estuarine stretches of Goa where observations are made. The bottom section represents the bathymetry of Mandovi-Zuari and surroundings (Dubey et al., 2019)

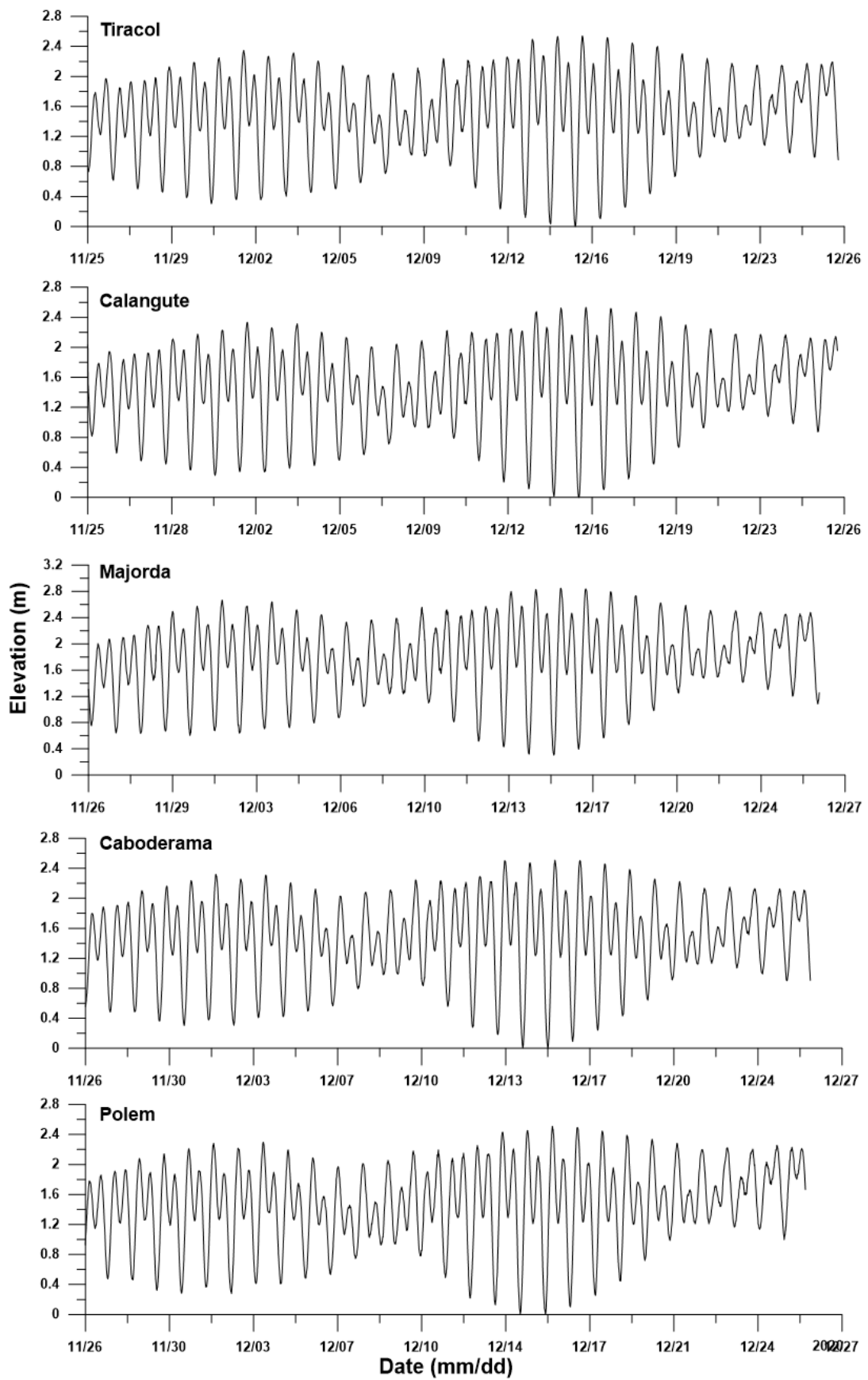


Fig. 2. Tide elevations at the coastal region during winter-monsoon

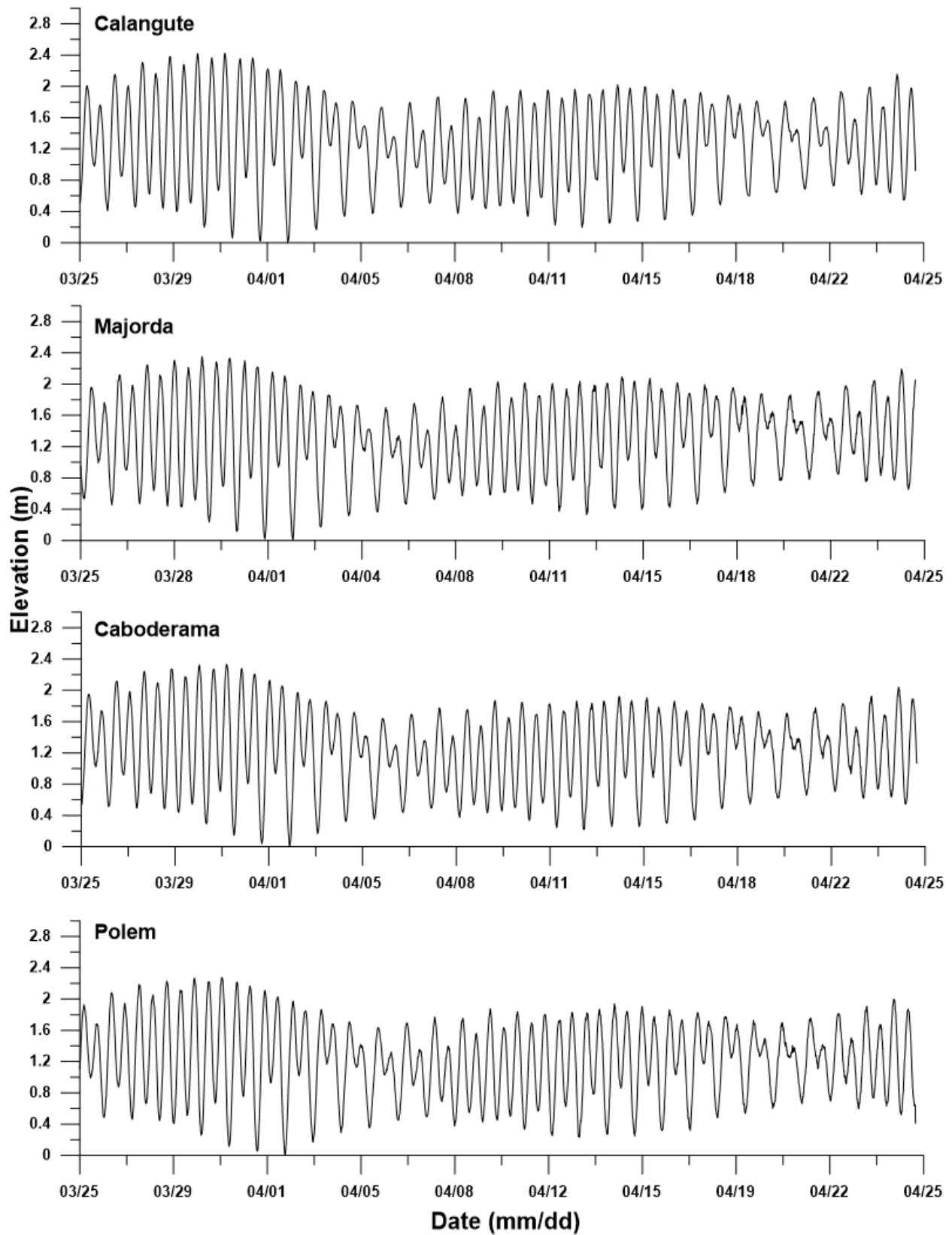


Fig. 3. Tide elevations at the coastal region during spring inter-monsoon

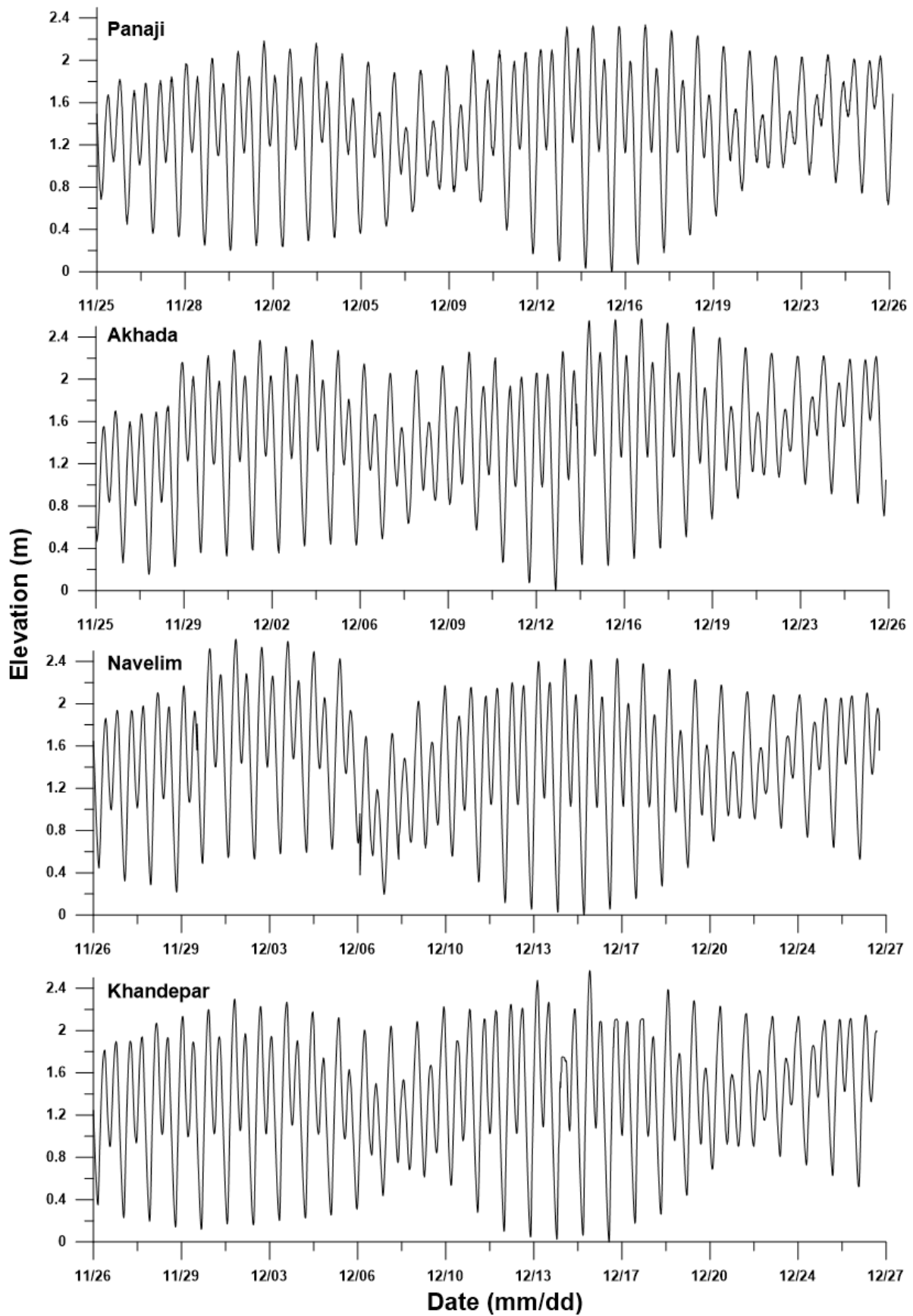


Fig. 4. Tide elevations inside Mandovi estuary during winter-monsoon

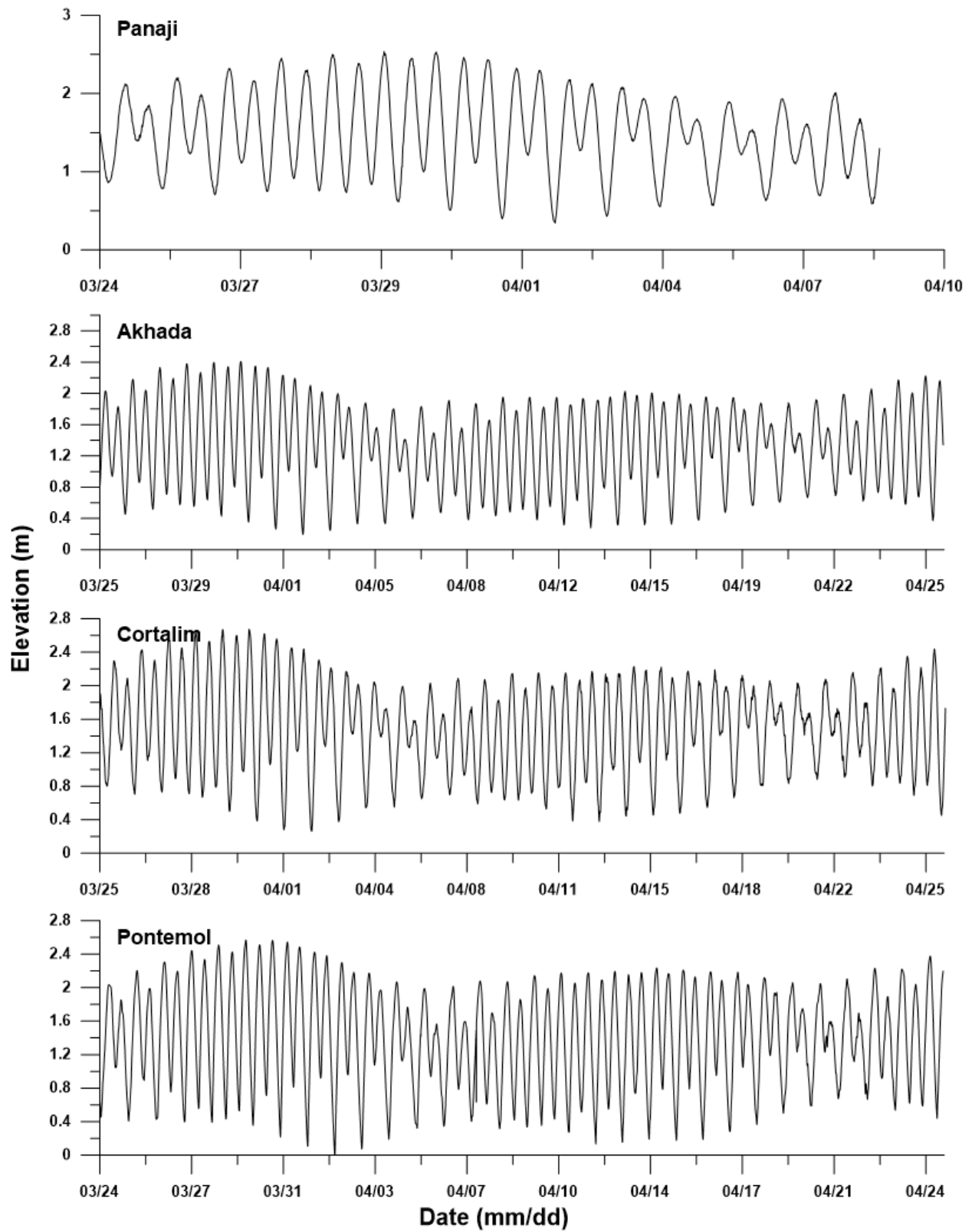


Fig. 5. Tide elevations inside Mandovi-Zuari estuarine channel during spring inter-monsoon

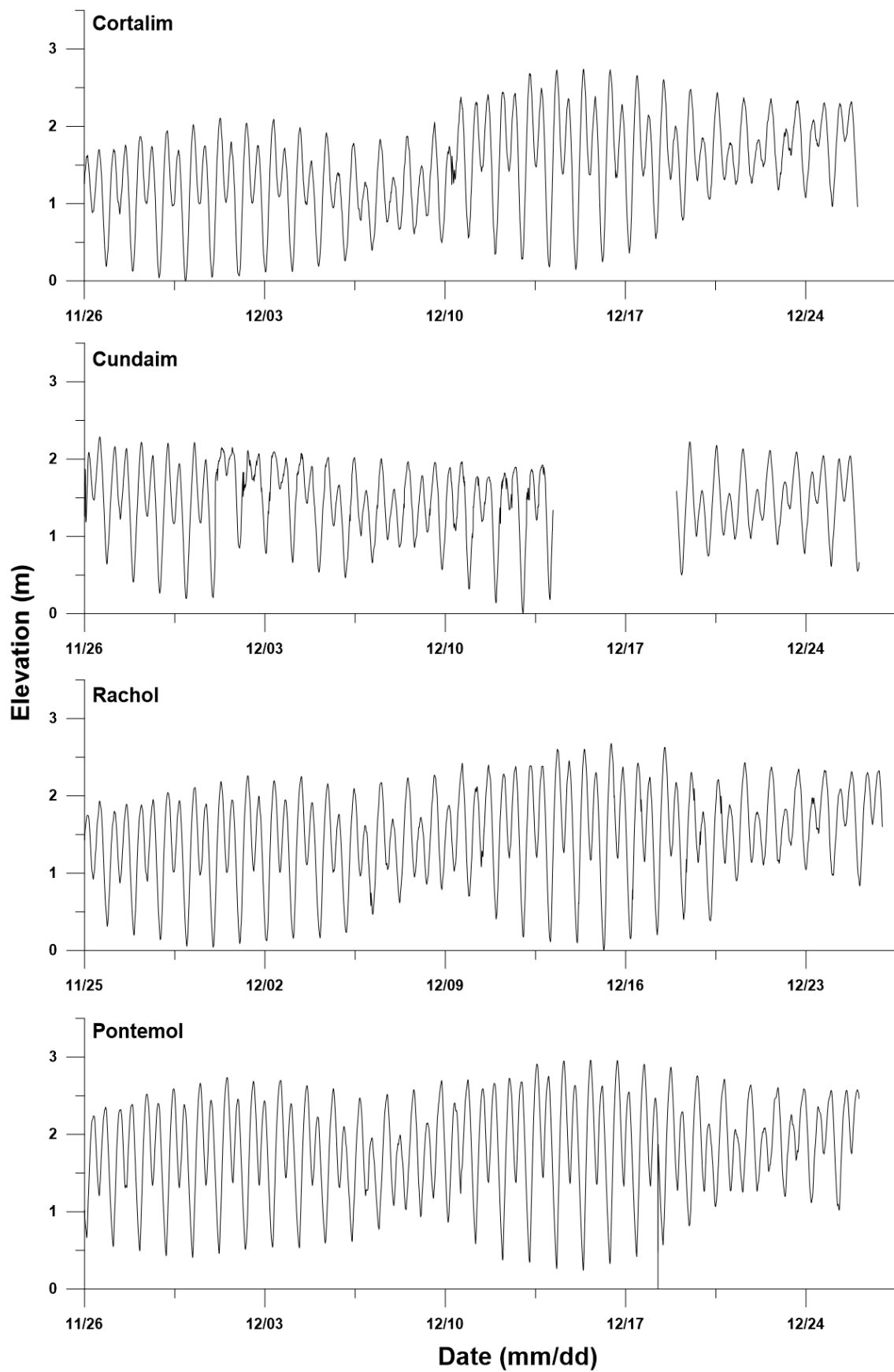


Fig. 6. Tide elevations inside Zuari estuary during winter-monsoon

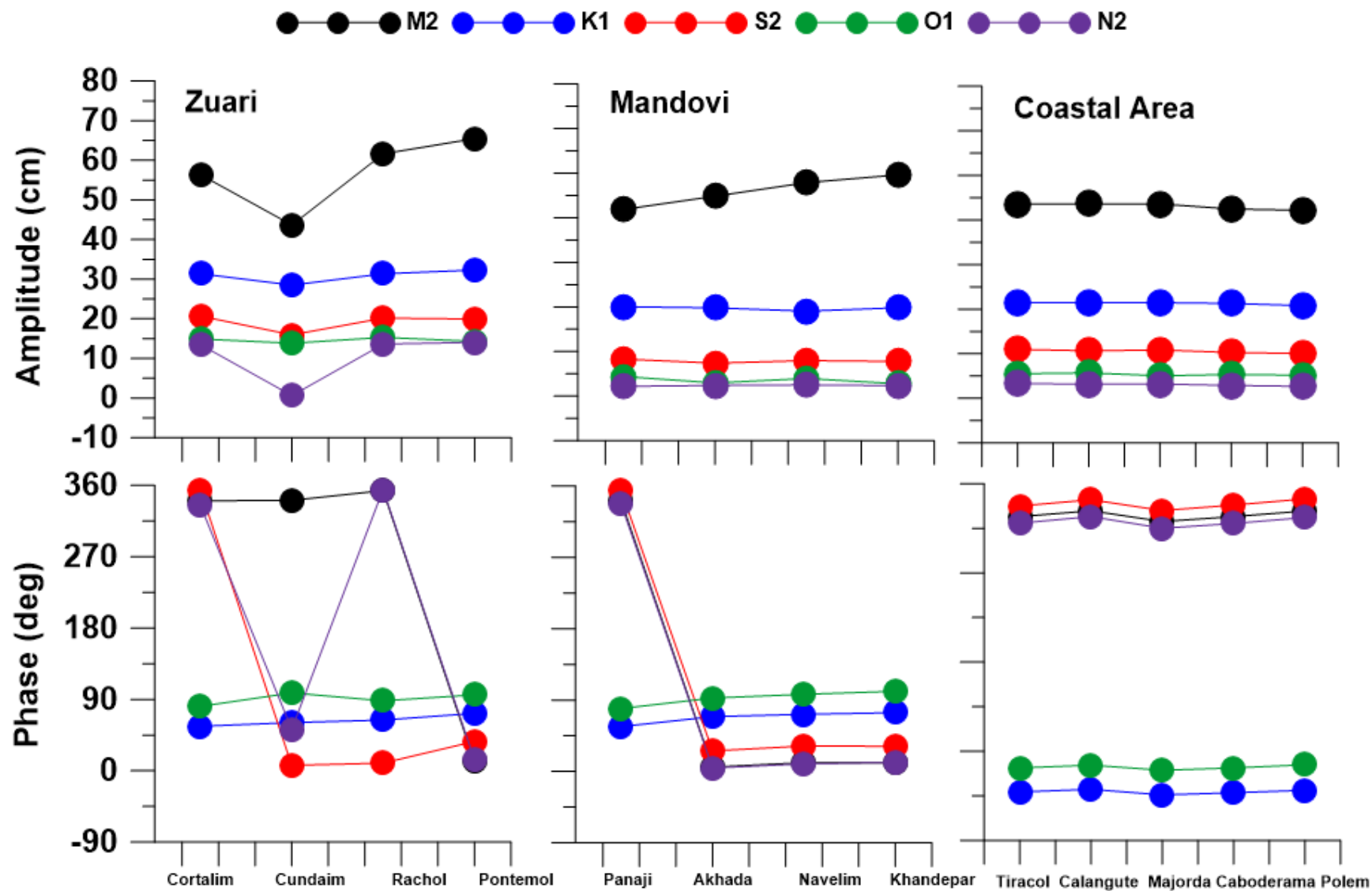


Fig. 7. Variations of amplitude and phase of the major tidal constituents at the selected locations during winter-monsoon

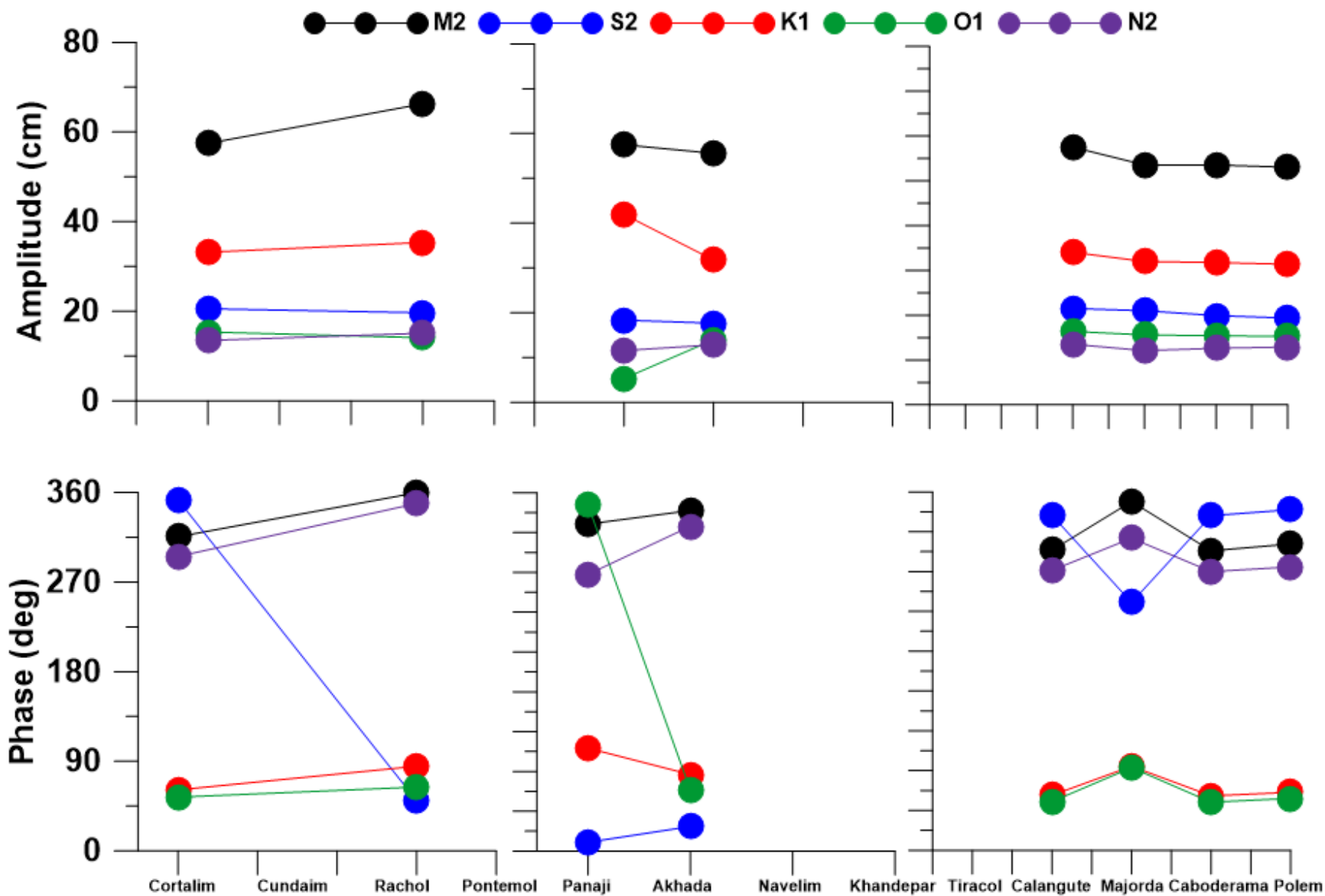


Fig. 8. Variations of amplitude and phase of the major tidal constituents at the selected locations during spring inter-monsoon

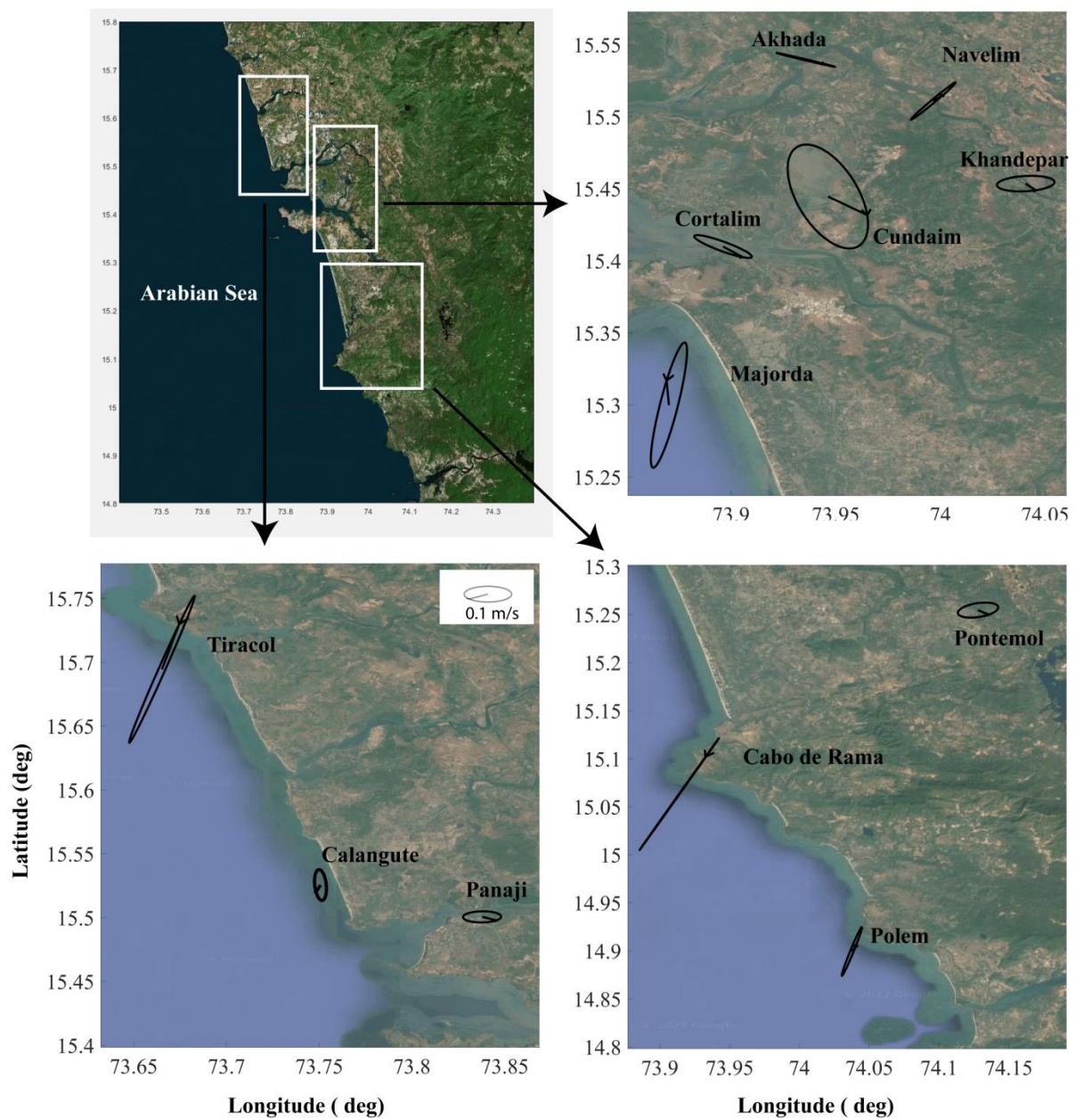


Fig. 9. Tidal ellipse plotted along the coastal and estuarine stretch of Goa

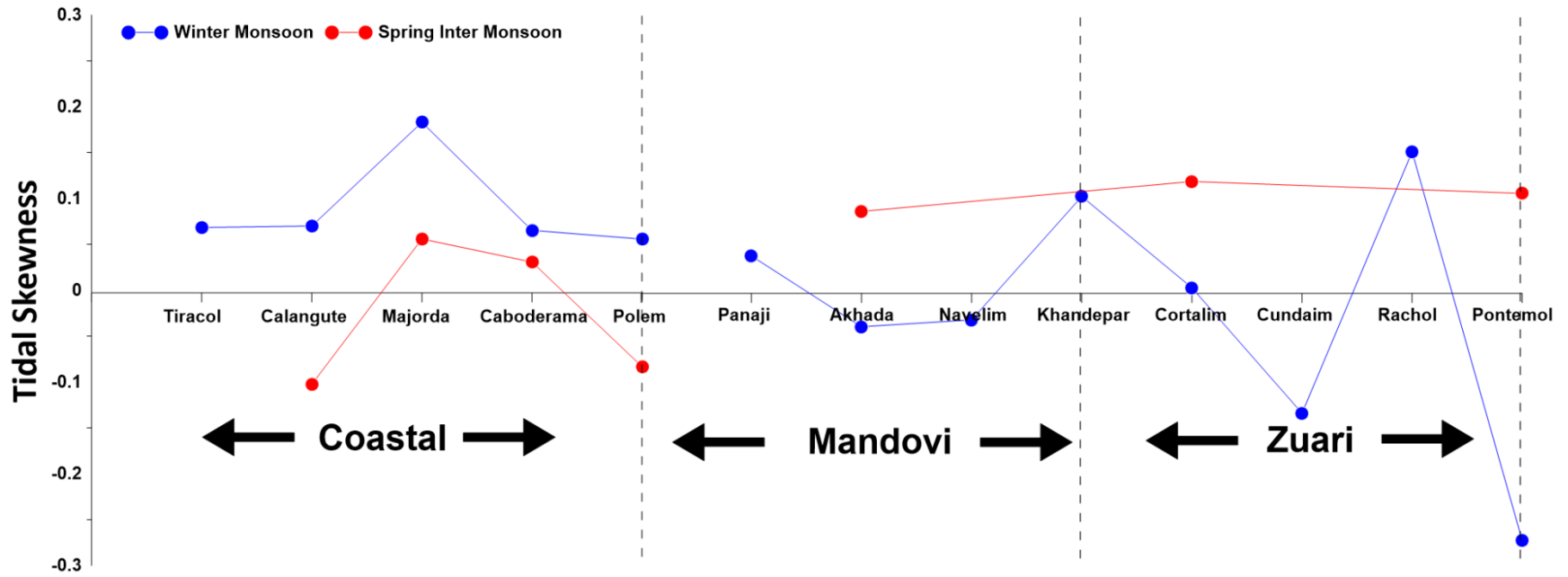


Fig. 10. Tidal skewness calculated for the coastal and estuarine stretch of Goa

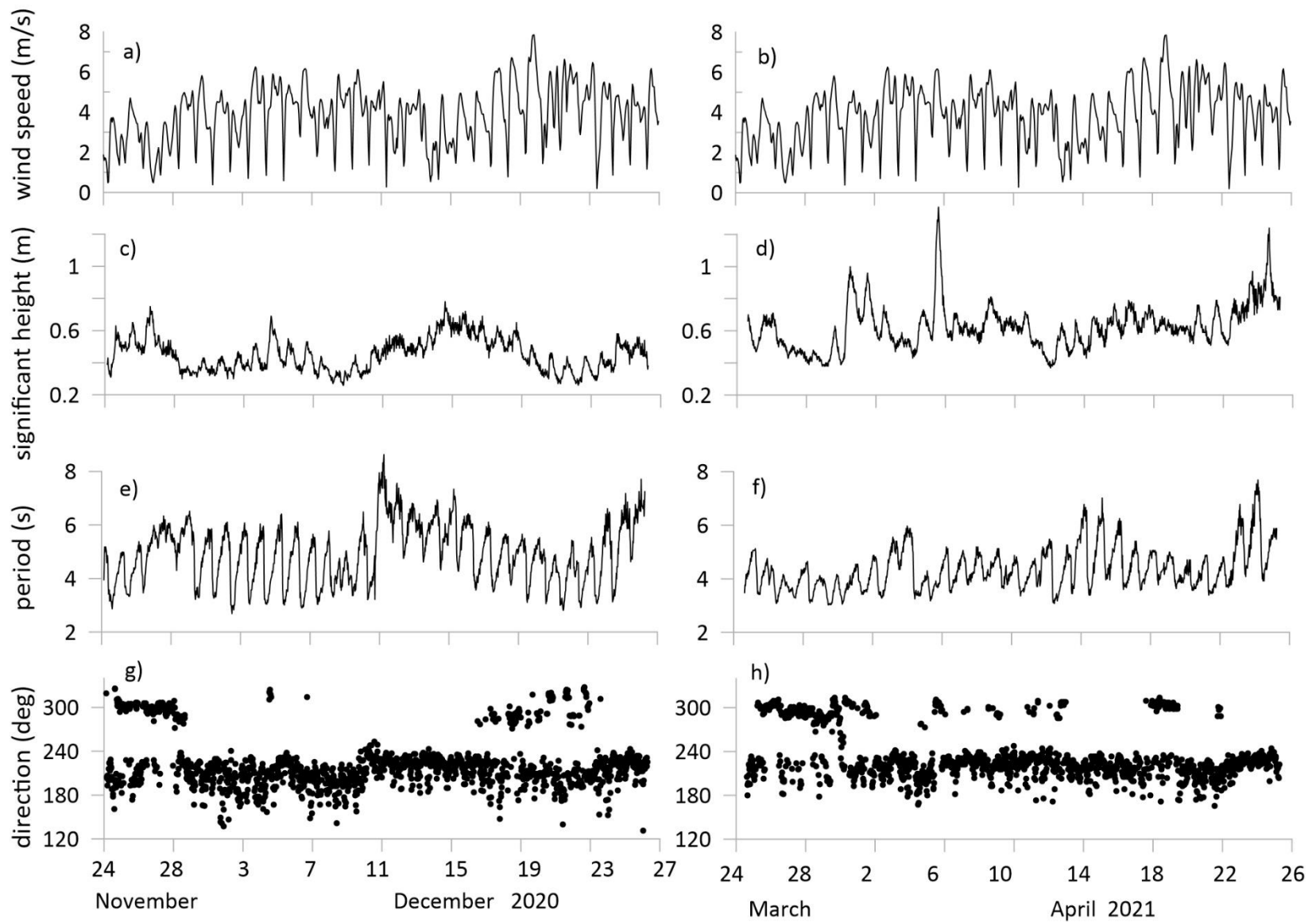


Fig. 11. a) and b) reanalysis wind data, c) and d) significant wave height, e) and f) mean wave period, g) and h) wave direction at Calangute. Left panel is for winter-monsoon and right panel is for spring inter-monsoon